Temporally and spatially resolved investigation of the $J = 0$–1 and $J = 2$–1, $3p$–$3s$ laser emissions in neonlike germanium

Yuelin Li,* Georg Pretzler, and Ernst E. Fill

Max-Planck-Institut für Quantenoptik, D-85748 Garching, Germany

Joseph Nilsen

Lawrence Livermore National Laboratory, Livermore, California 94550

Received April 18, 1995; revised manuscript received October 2, 1995

We report a time- and space-resolved investigation of the $J = 0-1$ and $J = 2-1$ lasers in neonlike germanium at 19.6, 23.2, and 23.6 nm. Germanium slabs were irradiated by the Asterix IV iodine laser at an intensity of approximately 2.0×10^{13} W cm^{-2} without and with a prepulse, which was 5.23 ns before the main pulse. The position of the lasing region was measured as a function of the prepulse intensity. It was found that lasing on the $J = 0-1$ transition at 19.6 nm occurs earlier in time and closer to the target surface than on the two $J = 2-1$ transisitions at 23.2 and 23.6 nm. The position for the 23.6-nm laser is the farthest from the target surface. A larger prepulse shifted all lasers farther from the target surface. Numerical simulations showed good qualitative agreement with experimental results when a prepulse was applied. For the case without a prepulse, calculations indicated the importance of beam refraction in modifying the effective gain of the soft-x-ray laser beam. © 1996 Optical Society of America

1. INTRODUCTION

Since the first demonstration of a high-gain soft-x-ray laser in an exploding foil target of selenium[1] and thereafter in a slab target of germanium[2] in neonlike ions, the puzzling behavior of the $J = 0-1$ transition (at 18.2 nm in selenium and 19.6 nm in germanium) in contrast to that of the $J = 2-1$ lasers has attracted both theoretical and experimental efforts for explanation. It has been predicted that the $J = 0-1$ line should have the most gain; but it has shown little or no gain, whereas the $J = 2-1$ lines have dominated the laser output in most experiments. Furthermore, in comparison with the $J = 2-1$ lasing, in previous experiments the $J = 0-1$ lasing was found to occur earlier and to undergo a larger refraction and a larger beam divergence.[3,4] These observations are partly explained by the suggestion that the $J = 2-1$ lasers are pumped mainly by recombination,[5,6] whereas the $J = 0-1$ laser is pumped predominantly by direct collisional monopole excitation from the ground state.

Recently efforts have succeeded, by various techniques, in enhancing the $J = 0-1$ laser or even in making it dominate the spectrum in selenium and elements with lower Z.[7–16] These techniques include the prepulse technique[7–12] (it is suspected that in Ref. 12 there was an undetected prepulse in the drive system[10]), the multipulse-plus-traveling-wave excitation technique,[13,14] and the use of curved targets.[15,16] These successes indicate the importance of hydrodynamics and beam optics in governing the anomalous behavior of the $J = 0-1$ transition. In these experiments the $J = 0-1$ lasing was again observed to occur earlier than the $J = 2-1$ lasing in nickel,[6] zinc,[10,12] germanium,[15,16] and selenium.[9] The different time histories suggest that the $J = 0-1$ and $J = 2-1$ laser emissions come from different plasma regions.

Motivated by these previous observations, we planned our experiments, aiming at a better understanding of the physics that drives each of these lasing lines. We chose germanium as the object of investigation because it is the element that has been investigated world wide in the past decade.[2–4,7,11,13,15–23] There are mainly five $3p-3s$ laser lines in neonlike germanium, i.e., one $J = 0-1$ transition at 19.6 nm, three $J = 2-1$ transitions at 23.2, 23.6, and 28.6 nm, and one $J = 1-1$ transition at 24.7 nm. In a recently published paper Murai *et al.*[4] systematically studied the properties of all five laser lines, focusing on their refraction properties. As a complement to their results, in the present paper we report a temporally and spatially resolved investigation of the 19.6, 23.2, and 23.6 nm laser lines by the prepulse technique. The position and the width of the lasing regions have been measured as a function of the prepulse intensity. It is found that the 19.6-nm lasing occurs closer to the target surface than the 23.2 and 23.6 nm lasing and that the 23.6 nm lasing region is the farthest from the target surface. A larger prepulse shifted all lasing regions away from the target surface. This is to our knowledge the first spatially resolved investigation of $J = 0-1$ versus $J = 2-1$ lasers in a slab target. An earlier spatially resolved experiment at the Lawrence Livermore National Laboratory showed the lasing region in a selenium exploding foil target to be symmetrical to the target center.[24] The different time histories of the 19.6, 23.2, and 23.6 nm lasing have also been measured. Numerical simulations showed a good qualitative agreement

0740-3224/96/040742-09$10.00

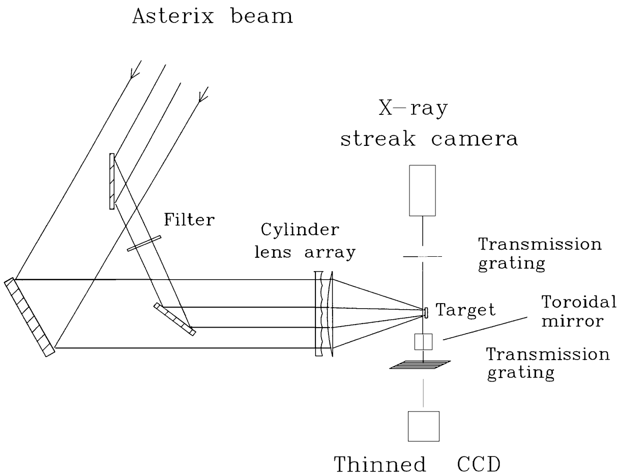

Fig. 1. Schematic overhead view of the experimental setup.

with experimental results when a prepulse was applied. For the case without a prepulse, calculations indicated the importance of beam refraction in modifying the effective gain of the soft-x-ray laser beam.

2. EXPERIMENTAL SETUP

The experiment was conducted at Max-Planck-Institut für Quantenoptik with the Asterix IV iodine laser.[25] A schematic overhead view of the experimental setup is shown in Fig. 1. Asterix IV is a one-beam facility; it delivers as much as 800 J at 1.315 μm with a pulse duration of 450 ps (FWHM). The spurious prepulse of the system was measured to be below 10^{-6} of the main pulse energy. A line focus was produced by a cylindrical-lens array consisting of six sections of cylindrical lenses.[26] Each section of the array generates a line focus 3 cm long and 30 μm wide; their overlap produces a line focus 150 μm wide and 3.0 cm long. To produce a defined prepulse, a setup similar to those of previous experiments was used,[10,11] in which a pair of 17.5-cm $\times$ 9-cm mirrors with 100% reflectivity at a 60° angle of incidence was inserted into the beam path before and after the final steering mirror, which deflects the beam by 60°. The delay between the main pulse and the prepulse was set to 5.23 ns. The maximum energy ratio of the prepulse to the main pulse is deduced from the area ratio of the prepulse mirrors to the Asterix beam cross section to be 15.1%; the ratio is variable by use of calibrated filters between the pair of prepulse mirrors without changing the energy in the main pulse. As the prepulse beam intersects only two sections of the cylindrical lens array, the line focus of the prepulse may be narrower than that of the main pulse, resulting in a higher intensity than that deduced from the energy ratio. The targets used were 2.4-cm- or 1.2-cm-long, 4-mm-thick planar germanium slabs with polished surfaces. The laser illuminated the slabs with the 3-cm-long line focus overfilling the target area. Typically a total energy (main pulse plus full prepulse) of 450 J was used.

The principal diagnostics were two transmission grating spectrometers. One of them was time integrated, spatially resolved, and coupled to a thinned, backside-illuminated CCD.[27] The diagnostic looked axially onto one end of the plasma column, with the spatial resolution in the direction perpendicular to the target surface. The spatial resolution was provided by a toroidal mirror with a magnification of ~2.6. The acceptance angle of the mirror was adjustable by a diaphragm. The spatial resolution was ~50 μm. A 5000 line/mm free-standing transmission grating with a 50-μm-wide slit dispersed the incident emission perpendicular to the spatially resolved direction. The wavelength coverage was 3.4–33.2 nm, with a spectral resolution of ~0.1 nm. The grating had a supporting structure perpendicular to the grating bars with a period of 4 μm that dispersed the incident emission along the spatial direction. This led to an additional spatial structure, which should be taken into account in the evaluation of the data.

On the other end of the axis a similar transmission grating was coupled to a streak camera[28] equipped with an optical CCD readout system (2DPC Image Analysis System, Hadland Photonics) with a time resolution of ~50 ps. The use of the CCD readout eliminates the need for a large image intensifier after the phosphorous screen of the streak camera. In this case the sensitivity of the system was found to be three times higher than a photographic film such as TMX. The use of the CCD readout eliminated the image distortion that would be caused by the large image intensifier used with film, and it gave better reproducibility, as the uncertainty inherent in developing film was also removed. Furthermore, the CCD provided a better dynamic range, which is ~10 times higher than that of film. With film or the CCD readout, the spatial resolution of the system was limited by the streak camera itself to be 125 μm.[28] The 150-μm slit on the grating was oriented parallel to the target surface and was 83 cm away from the target; therefore the spectrometer covered only a small angular range. In the experiment the grating and the streak camera could be translated in the direction of the angular resolution to meet the maximum laser output. The 1.8 cm $\times$ 300 μm slit on the photocathode was horizontally placed and covered a wavelength range of ~40.0 nm with a resolution of 1 nm. The cathode is 0.11 μm of CsI on a 0.11-μm-thick carbon substrate.

3. EXPERIMENTAL RESULTS

Experiments were done with 0%, 1.5%, and 15% prepulses. As has been reported previously for germanium and zinc, without a prepulse the $J = 0{-}1$ transition lased weaker than the $J = 2{-}1$ lasers or did not lase at all.[7,10–12] When a prepulse was applied, the $J = 0{-}1$ laser emission dominated the spectrum, and the $J = 2{-}1$ laser emissions were also enhanced.[10–12] In this experiment the effective time-integrated gains of the 19.6-, 23.2-, and 23.6-nm laser emissions in germanium were measured to be 3.7, 2.7, and 3.1 cm^{-1} with a 1.5% prepulse.

Figure 2(a) gives a streaked spectrum for a 2.4-cm germanium target taken at 7 mrad from the axis with a 1.5% prepulse. The $J = 0{-}1$ and $J = 2{-}1$ laser lines at 19.6, 23.2, and 23.6 nm are seen to dominate the spectrum (the 23.2- and 23.6-nm laser lines are not resolved). The other $J = 2{-}1$ laser line at 28.6 nm is barely visible. The 19.6-nm laser emission is seen to occur considerably earlier than the pair of $J = 2{-}1$ laser emissions at 23.2

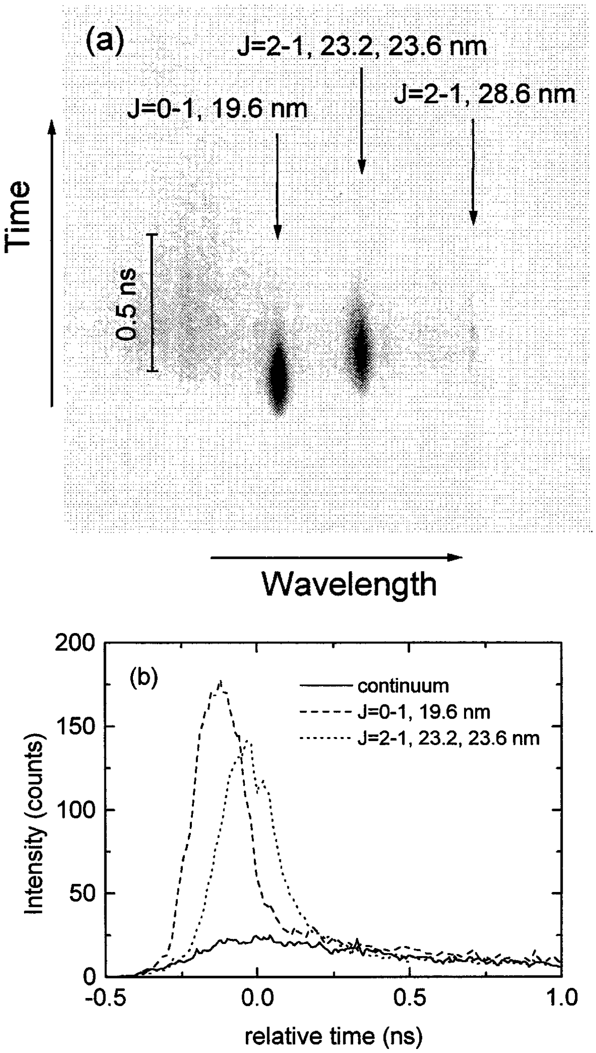

Fig. 2. (a) Record of the streak camera for a 2.4-cm-long germanium target obtained 7 mrad off axis. The two $J = 2-1$ lines at 23.2 and 23.6 nm are not resolved owing to the low wavelength resolution. One can clearly see that the $J = 0-1$ transition at 19.6 nm occurs earlier than the $J = 2-1$ transitions. The other $J = 2-1$ line, at 28.6 nm, is also barely seen. A driving energy of 493 J was used with a 1.5% prepulse. (b) Traces along the time direction for the 19.6-nm laser and the pair of lasers at 23.2 and 23.6 nm from (a). The zero time is set at the maximum of the continuum emission, which corresponds approximately to the peak of the drive pulse. The 19.6-nm laser rises more rapidly and peaks ~100 ps earlier than the 23.2 and 23.6 nm lasers and the continuum emission.

and 23.6 nm. In Fig. 2(b) we show the traces along the time direction of Fig. 2(a) taken at the maximum of the 19.6- and 23.6-nm laser lines. The 19.6-nm laser line is observed to peak ~100 ps earlier with a steeper leading edge than the 23.2 and the 23.6 nm laser lines. This observation agrees with the previously reported results with or without a prepulse, as well as with the observation with the curved targets for a number of elements.[3,4,7,9,10,12,15,16] The different time histories suggest that, as has been mentioned by several authors,[7,10,12] different laser lines come from different regions in the plasma.

Although we did not measure the dependence of the timing of the lasing on the prepulse intensity, our simulation suggests that the delay between the peaks of the $J = 0-1$ and the $J = 2-1$ lasing, as well as the optical drive pulse, varies as the intensity of the prepulse changes. A further experiment for measuring the detailed temporal behavior of the lasing is under way.

The time-integrated but spatially resolved spectrum corresponding to Fig. 2 is given in Fig. 3(a), in which the spatial direction designated is along the normal of the target surface. A 1.5-μm aluminum filter was used to attenuate the laser intensity. The strong lasing at 19.6, 23.2, and 23.6 nm, accompanied by diffraction caused by the support structure of the grating, is clearly seen to dominate the spectrum. The central spots give the spatial positions of the lasing, while the adjacent spots in the spatial direction are the high-order diffraction pattern of the support. The other laser lines at 24.7 and 28.6 nm are barely seen. One can see that the diffraction pattern overlaps slightly with the central spot at 19.6 and 23.6 nm; this is due to the display scaling selected for showing the weak laser at 28.6 nm, and therefore the strong 19.6 and 23.6 nm lasers and their ±first-order diffraction are saturated. However, the diffraction pattern does influence our spatial resolution.

To ensure that the x-ray laser beam is completely collected, a large aperture for the imaging optics of 20 mrad was used for this shot in Fig. 2. In this case, owing to the short depth of focus of the imaging optics, it is difficult to determine the exact position of the target surface, and therefore we were not able to measure the positions of the lasing regions, although they seem to be well imaged according to the relatively small divergence of the laser beams. However, one can still see that the 19.6-nm laser line and the pair of 23.2 and 23.6 nm laser lines peak at different positions. In Fig. 3(b) we show the trace along the spectral direction taken at the maximum of the 19.6-nm laser line. All five laser transitions are clearly seen, and the laser line at 19.6 nm dominates (note the log scale).

In a long target, besides the difficulty in determining the position of the target surface, the refraction of the laser beam along the target normal also makes it difficult to determine the original lasing region. The shift of the lasing position from the target surface with increasing target length has been observed for the $J = 0-1$, 25.5-nm lasing in neonlike iron.[29] To overcome these problems, we used 1.2-cm-long targets to reduce the refractive effect and limited the acceptance aperture to ~5 mrad to increase the depth of focus of the imaging system. However, there are still some refractive effects that influence the spatially resolved measurements, as is discussed in Section 4.

Under these conditions the positions and the widths of the lasing region were measured for 0%, 1.5%, and 15% prepulses. Figures 4(a), 4(b), and 4(c) summarize the measurement of the intensity distribution of the 19.6, 23.2, and 23.6 nm lasers along the spatial direction. The target surface is defined as position zero, which was determined as the crossing point obtained by extrapolating the straight part of the rear slope (of a background trace close to the laser) down to zero intensity. The error induced in this way was ~50 μm. The curves displayed in Figs. 4(a), 4(b), and 4(c) are corrected for the background and therefore represent the emission from laser transitions alone. This permits a direct comparison with the

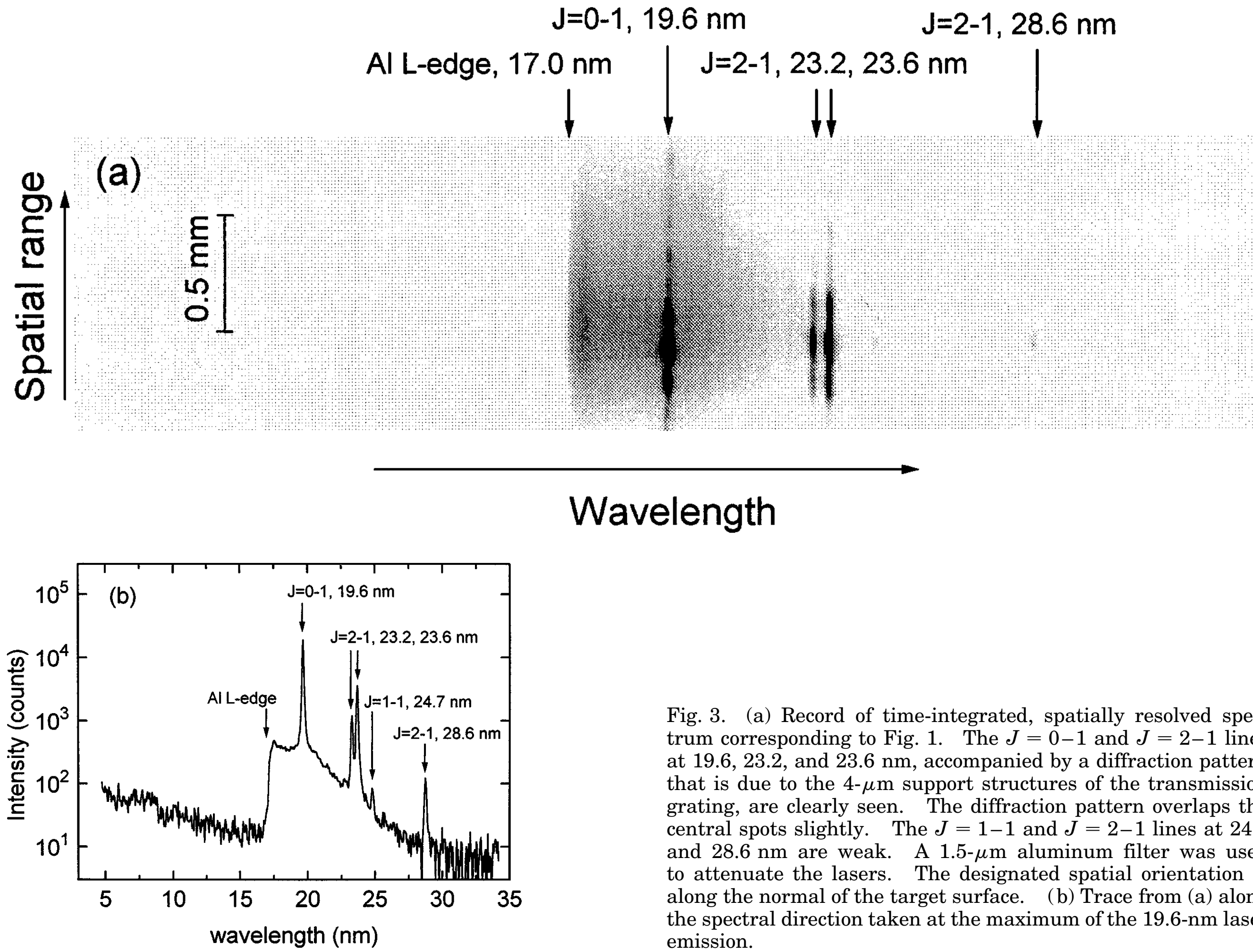

Fig. 3. (a) Record of time-integrated, spatially resolved spectrum corresponding to Fig. 1. The $J = 0-1$ and $J = 2-1$ lines at 19.6, 23.2, and 23.6 nm, accompanied by a diffraction pattern that is due to the 4-μm support structures of the transmission grating, are clearly seen. The diffraction pattern overlaps the central spots slightly. The $J = 1-1$ and $J = 2-1$ lines at 24.7 and 28.6 nm are weak. A 1.5-μm aluminum filter was used to attenuate the lasers. The designated spatial orientation is along the normal of the target surface. (b) Trace from (a) along the spectral direction taken at the maximum of the 19.6-nm laser emission.

simulated results in Figs. 4(d), 4(e), and 4(f), in which the spatial profile of the gain coefficients, time integrated from -0.3 to 0.7 ns around the peak of the main pulse, are given. A detailed discussion of the simulation will be found in Section 4. As detailed structures in the lasing region cannot be resolved, only the peak position and the widths of the lasing region were measured.

Although diffraction from the supporting structure influences the spatial profile, one can see in Fig. 4 that the 19.6-nm laser emission has a maximum closest to the target surface (zero coordinate) as compared with the 23.2 and 23.6 nm laser emissions. For example, with a 1.5% prepulse [Fig. 4(b)] the 19.6-nm laser emission peaks at $\sim$137 μm, and the 23.2- and the 23.6-nm laser emissions peak at 162 and 172 μm from the target surface, respectively. Also, the region of the 19.6-nm laser emission is slightly narrower. With an increased prepulse intensity all lasing occurs farther from the target surface, and the lasing regions become broader. For the 19.6-nm laser emission without a prepulse, the lasing region is $\sim$70 μm wide (FWHM), and it increases to $\sim$100 μm when a 1.5% or a 15% prepulse is used. The width of the 23.6-nm laser region changes from 70 to 120 to 160 μm as the prepulse changes from 0 to 1.5 to 15%, respectively. These values are certainly influenced by the diffraction pattern of the grating support, which broadened the apparent widths of the lasing regions. Therefore the values represent the upper limits of the actual widths of the lasing regions. The peak lasing positions summarized from Fig. 4 are given in Table 1. Also given in Table 1 are the peak positions of the time-integrated gain from the simulation.

Our measurements explain why the previously measured divergence and refractive angle for the 19.6-nm laser emission are larger than for the 23.2 and 23.6 nm laser emissions. As the 19.6-nm lasing occurs earlier and originates closer to the target surface, where the electron density is higher and the density gradient is larger, a larger refraction is induced. When the refraction of the laser beam dominates the beam propagation, the effective gain–length product will be considerably reduced.

4. SIMULATIONS AND DISCUSSION

To model these experiments, we performed LASNEX one-dimensional simulations.[30] The prepulse and the main pulse are assumed to be Gaussian pulses with a FWHM duration of 450 ps and are focused to a width of 150 μm to yield a peak intensity of 1.9×10^{13} W cm^{-2} on target, similar to the experimental conditions. The size of the prepulse is varied from 0% (no prepulse) to 1.5% to 15% of the main pulse, which is 380 J. The LASNEX calculations included an expansion angle of 15° in the dimension perpendicular to the primary expansion so as to simu-

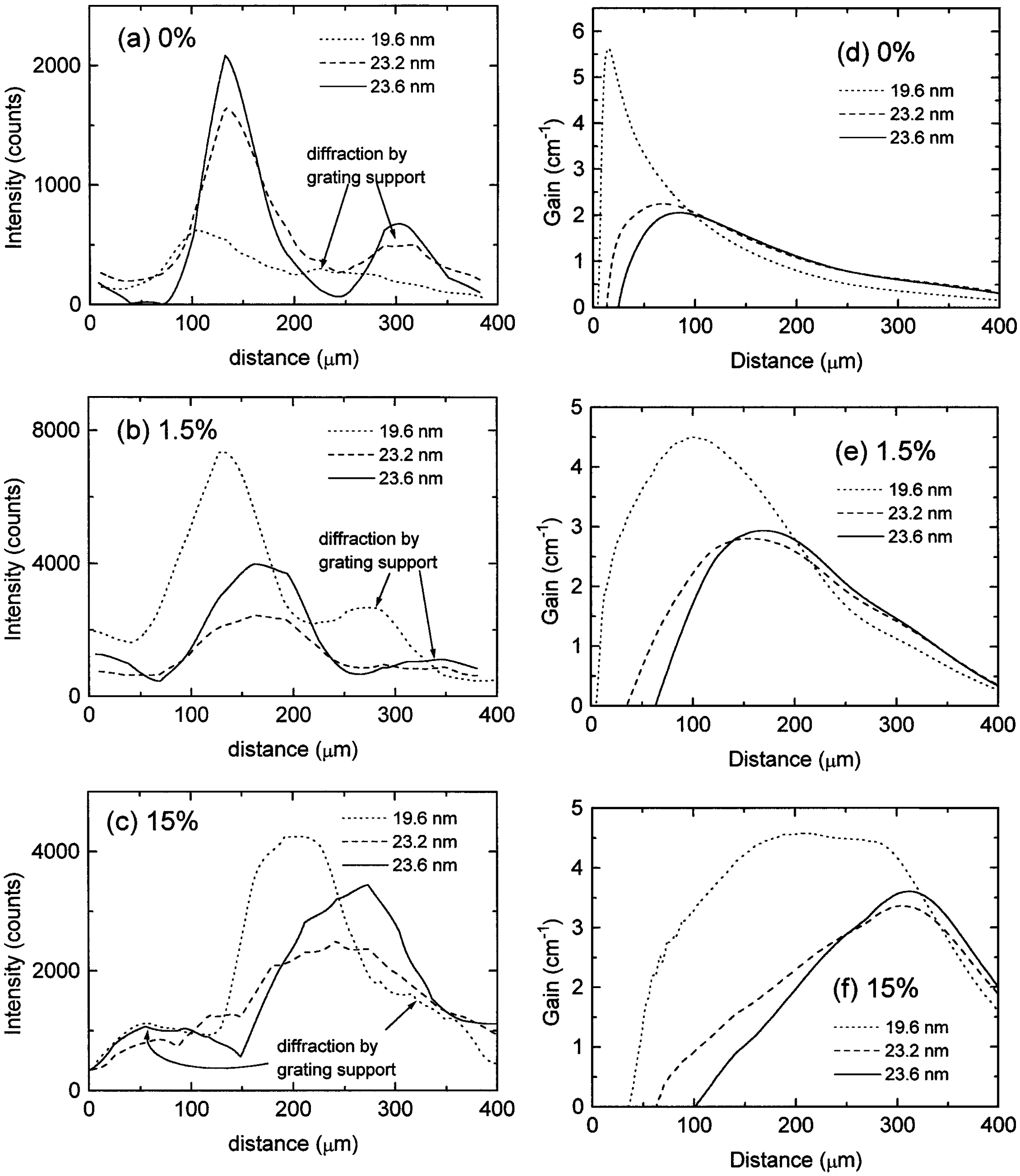

Fig. 4. Spatial distribution of the 19.6, 23.2, and 23.6 nm laser emissions measured for 12-mm targets with (a) no prepulse, (b) a 1.5% prepulse, and (c) a 15% prepulse. Also given are the calculated spatial profiles of the gain coefficients, time integrated from −0.3 to 0.7 ns around the peak of the main pulse, with (d) no prepulse, (e) a 1.5% prepulse, and (f) a 15% prepulse. The energy in the main pulse was kept at 380 J in both experiments and simulations. Note that the intensity scales for (a), (b), and (c) are comparable.

late two-dimensional effects. With the LASNEX calculated densities, temperatures, and velocities used as input to the XRASER code,[31] the gains of the laser lines were calculated including radiation-trapping effects on the $3s$–$2p$ transitions in neonlike germanium. Bulk Doppler effects due to the expansion of the plasmas were also included.

Figures 5(a), 5(b), and 5(c) plot contours of the gain versus space and time for the $J = 0$–1 line at 19.6 nm for the three cases of no prepulse, a 1.5% prepulse, and a 15% prepulse, respectively. The surface of the target is at distance zero. The peak illumination is set at time zero for all three cases. Contours represent 12% changes from the darkest region, which has a gain greater than 14 cm^{-1}. Figures 6 and 7 plot similar contours for the 23.2 and 23.6 nm lines, respectively, for the three cases. Contours are still 12% changes, but now the darkest region has a gain greater than 7.5 cm^{-1}.

For all three laser lines one notices that the gain region moves farther from the surface as the prepulse is increased. There is a big qualitative difference between the 19.6-nm line and the other two lines. The 23.2 and the 23.6 nm lines have their peak gains far from the surface, near the time of peak optical illumination. Figures 5, 6, and 7 are integrated over a period of −300

Table 1. Comparison of the Measured Positions of Peak Intensity (x_{exp}) and Calculated Peak-Gain Positions (x_{calc}) for the 19.6-, 23.2-, and 23.6-nm Lasing Lines for the 0%, 1.5%, and 15% Prepulse Cases[a]

Lasing Transition (nm)	Prepulse Level (%)	x_{exp} (μm)	x_{calc} (μm)
19.6	0	114	15
	1.5	137	102
	15	212	225
23.2	0	132	69
	1.5	162	157
	15	247	305
23.6	0	132	86
	1.5	172	170
	15	273	311

[a]An error bar of ± 50 μm is estimated for the experimental values.

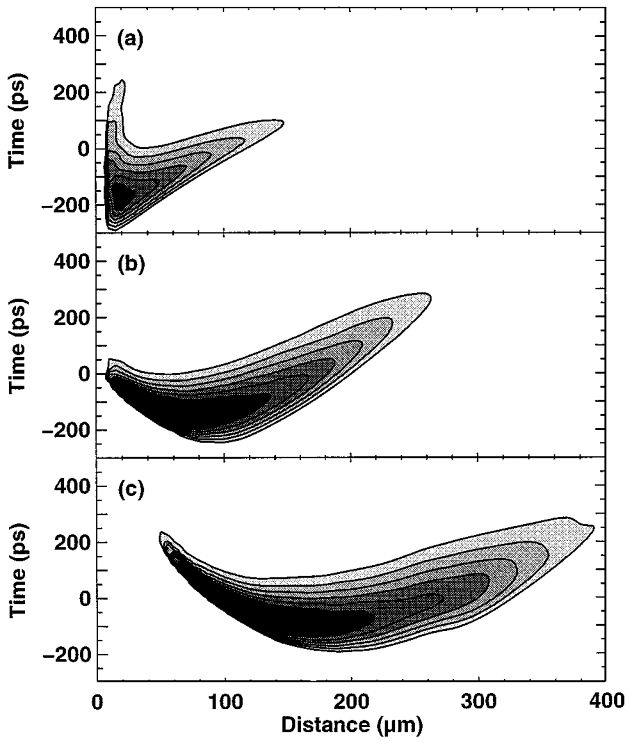

Fig. 5. Contours of gain versus space and time for the $J = 0-1$, 19.6-nm laser line as calculated by the XRASER code with the hydrodynamic simulations from LASNEX used as input. In the three cases shown the prepulse varies from (a) 0% to (b) 1.5% to (c) 15% of the main pulse, which is held constant at 380 J. Contours represent 12% changes, with the darkest region having a gain greater than 14 cm^{-1}. The main pulse peaks at time zero for all three cases.

to 700 ps to yield time-integrated spatial distributions of the gain, which are presented in Figs. 4(d)–4(f). The peak gain positions are given in Table 1. Except for the case of no prepulse, good qualitative agreement with the measured peak position of lasing emission can be seen in Table 1 and Fig. 4. However, measuring the peak laser emission is quite different from measuring the position of peak gain because of refraction effects and the exponential dependence of the intensity on the gain coefficient. Refraction effects also reduce the gain measured in the experiment, which could explain the factor of 3 or 4 difference between our simulated gains and the measured gains, e.g., for the 1.5% prepulse case. The effect of beam refraction on modifying the effective gain measured has recently been studied numerically.[32]

Figure 8 shows contours of the log of the electron density versus space and time for the three cases. The black region represents an electron density greater than the critical density of 6.4×10^{20} cm^{-3}, and each contour represents a change of 0.1 in the log, or an approximately 21% lower density. Clearly the gradient in the electron density is much larger for the no-prepulse case as compared with the two-prepulse cases. For example, consider how far an x ray traveling parallel to the target surface is refracted away from the surface after traveling 1.2 cm if the beam is subject to a constant gradient in the electron density. The refracted distance x is given by

$$x = \frac{\mathrm{d}n}{\mathrm{d}x}\frac{z^2}{2},$$

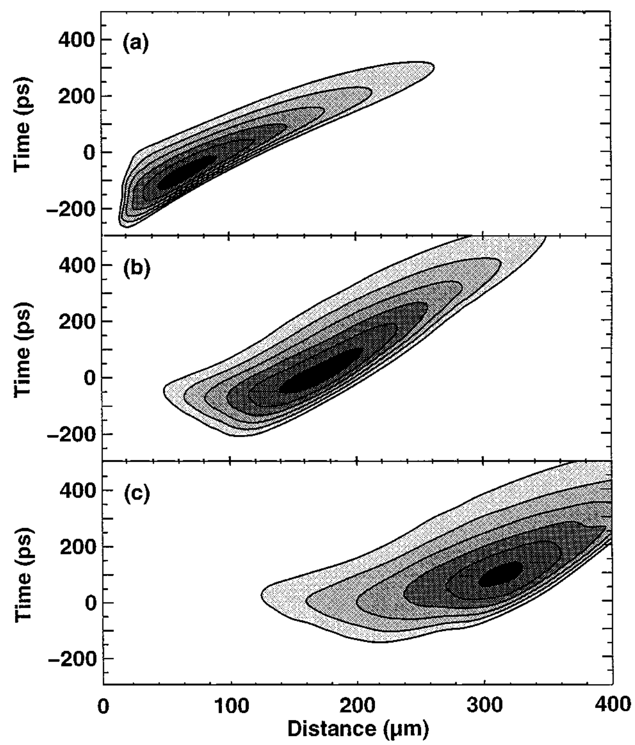

Fig. 6. Contours of gain versus space and time for the $J = 2-1$ laser at 23.2 nm as calculated by the XRASER code with the hydrodynamic simulations from LASNEX used as input. In the three cases shown the prepulse varies from (a) 0% to (b) 1.5% to (c) 15% of the main pulse, which is held constant at 380 J. Contours represent 12% changes, with the darkest region having a gain greater than 7.5 cm^{-1}. The main pulse peaks at time zero for all three cases.

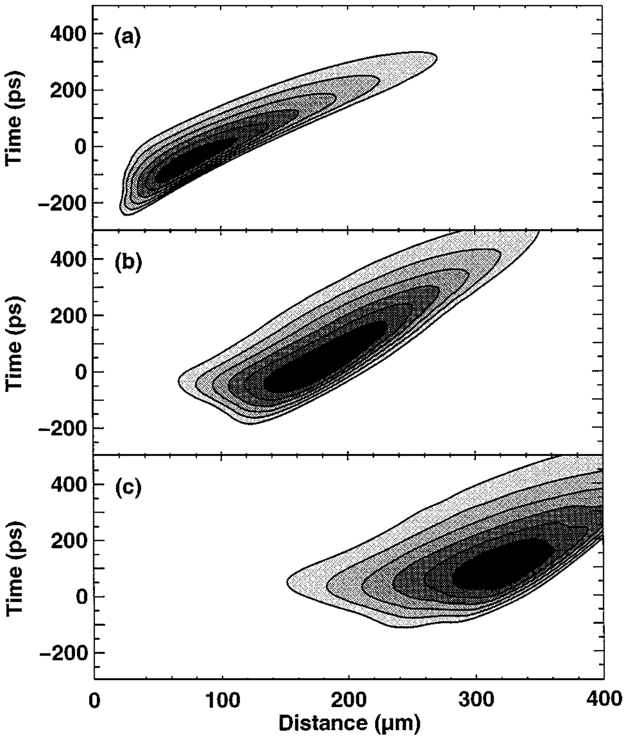

Fig. 7. Contours of gain versus space and time for the $J = 2-1$ laser at 23.6 nm as calculated by the XRASER code with the hydrodynamic simulations from LASNEX used as input. In the three cases shown the prepulse varies from (a) 0% to (b) 1.5% to (c) 15% of the main pulse, which is held constant at 380 J. Contours represent 12% changes, with the darkest region having a gain greater than 7.5 cm^{-1}. The main pulse peaks at time zero for all three cases.

where z is the propagation distance, 1.2 cm in this case, and dn/dx is the gradient in the refractive index. The gradient dn/dx is related to the gradient in the electron density by

$$\frac{dn}{dx} = -4.485 \times 10^{-28} \lambda^2 \frac{dn_e}{dx},$$

where the wavelength λ is in nanometers and the electron density gradient dn_e/dx is in electrons per centimeters to the fourth power.

For the 23.6-nm laser line in the 1.5% prepulse case, the gain peaks at 8.8 cm^{-1}, at 180 μm, at 35 ps. At this position the electron density $n_e = 1.3 \times 10^{20}$ cm^{-3}, the electron temperature $\theta_e = 1.05$ keV, and the gradient in the electron density $dn_e/dx = -1.4 \times 10^{22}$ cm^{-4}. A 23.6-nm x ray is refracted by 25 μm after traveling 1.2 cm. Given the 120-μm measured width for the emission region, the x ray experiences gain down the entire length of the 1.2-cm-long x-ray laser targets used in these experiments. In contrast, for the no-prepulse case, the gain peaks at 8.4 cm^{-1}, at 72 μm, at −60 ps. Here $n_e = 1.6 \times 10^{20}$ cm^{-3}, $\theta_e = 0.83$ keV, $dn_e/dx = -5.7 \times 10^{22}$ cm^{-4}, and the same x ray would be refracted by 100 μm after 1.2 cm. Since the laser emission region is measured to be 70 μm, even for this short sample, the laser is refracted out of the gain region before it can exponentiate down the full length of the target. So, even though the peak gains are similar for the three cases, the no-prepulse case cannot utilize the full gain because of refraction limitations. The situation for the 23.2-nm line is similar to that of the 23.6-nm line except that the gain is ~10% smaller and the refractive index is 3% smaller.

For the 19.6-nm line the refraction effect is much more severe, which is no doubt the reason that this line was not observed in the early neonlike selenium experiments.[1] Now the region of high gain extends close to the target surface, where the electron density is very high, even above critical density, and the gain occurs before the peak of the optical illumination. By observation of the electron density in Fig. 8, it is clear that most of the high-gain region has too large a gradient in the refractive index to allow for any substantial propagation. For the no-prepulse case, the gain peaks at 15 cm^{-1}, at 17 μm from the surface, at −160 ps. Here $n_e = 7.3 \times 10^{20}$ cm^{-3}, $\theta_e = 0.61$ keV, and $dn_e/dx = -5.4 \times 10^{23}$ cm^{-4}. An x ray traveling parallel to the surface would be refracted by 670 μm after traveling 1.2 cm. Looked at another way, the x ray could travel only 0.2 cm before it would be refracted out of the 20-μm-wide gain region. Clearly, no lasing will be seen under these conditions. It is only later in time, when the gradients and gain are smaller, that there will be any chance for significant laser propagation through the gain region.

Even with the prepulse, the region of peak gain for the 19.6-nm line is close to the target surface. However, the high-gain region extends much further out and reaches into regions where the gradients are much smaller. For

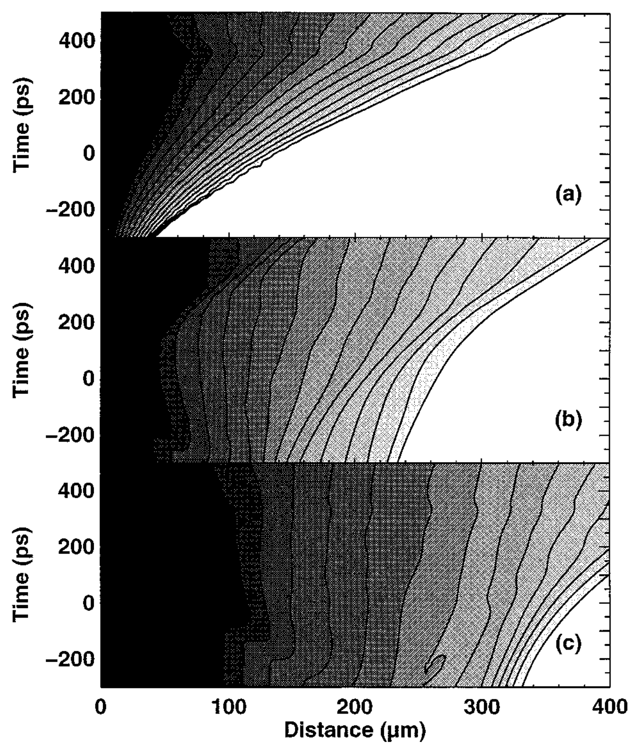

Fig. 8. Contours of electron density versus space and time, calculated by hydrodynamic simulations from LASNEX. In the three cases shown the prepulse varies from (a) 0% to (b) 1.5% to (c) 15% of the main pulse, which is held constant at 380 J. Contours are in $\log(n_e)$, with the darkest region being 20.8, corresponding to the critical density of 6.4×10^{20} cm^{-3}, and goes in a step of 0.1 or approximately 21% lower density down to 19.5, corresponding to a density of 3×10^{19} cm^{-3}. The main pulse peaks at time zero for all three cases.

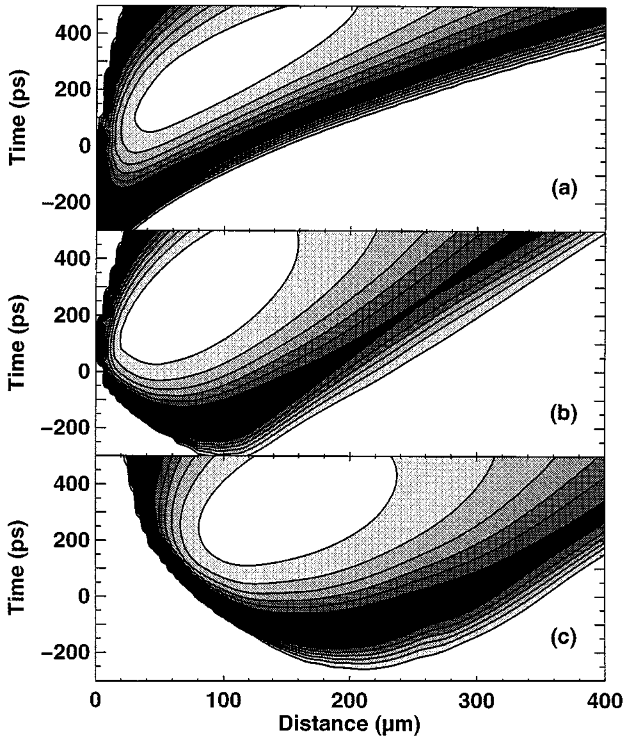

Fig. 9. Contours of neonlike fraction versus space and time as calculated by the XRASER code with the hydrodynamic simulations from LASNEX used as input. In the three cases shown the prepulse varies from (a) 0% to (b) 1.5% to (c) 15% of the main pulse, which is held constant at 380 J. Contours represent 8% changes in the neonlike fraction with the darkest region having neonlike fraction greater than 50%. The white regions have neonlike fraction less than 10%. The main pulse peaks at time zero for all three cases.

example, consider now the edge of the highest-gain region furthest from the surface. For the 1.5% prepulse case, we calculate a gain of 13.9 cm^{-1} at 137 μm and −85 ps. The electron density $n_e = 1.9 \times 10^{20}\ \mathrm{cm}^{-3}$, $\theta_e = 0.89$ keV, $\mathrm{d}n_e/\mathrm{d}x = -2.2 \times 10^{22}\ \mathrm{cm}^{-4}$, and the x ray would be refracted by 27 μm after 1.2 cm. For the 15% prepulse case we have gain of 13 cm^{-1} at 221 μm and −75 ps with $n_e = 2.2 \times 10^{20}\ \mathrm{cm}^{-3}$, $\theta_e = 0.78$ keV, and $\mathrm{d}n_e/\mathrm{d}x = -2.0 \times 10^{22}\ \mathrm{cm}^{-4}$. The x-ray is refracted only 25 μm after 1.2 cm.

In Fig. 4 and Table 1 for the 19.6-nm line good qualitative agreement between the calculations and the experiments is seen except for the no-prepulse case, for which the refraction effect is much larger and the laser emission is weighted by regions farther from the surface with lower gradients and smaller gains to let us use the entire length of the laser plasma effectively. The laser emission will appear farther from the surface than the peak gain in all these cases, since the electron density is smaller as you move away from the surface and the x rays bend away from the solid surface under these conditions. In the future we plan to combine plasma modeling with beam-propagation calculations to estimate the space- and time-dependent laser emission under these experimental conditions.

If we look at the time histories of the laser lines shown in Figs. 5–7, we see that the 19.6-nm line peaks 120 ps before the 23.2 and 23.6 nm lines for the 1.5% prepulse case, which is in good agreement with the 100-ps delay observed experimentally. This delay between the gains of the different lines can be explained by examination of the ionization balance. Figure 9 shows the neonlike fraction versus space and time for the three prepulse cases. The darkest region has a neonlike fraction of greater than 50%, and each lighter contour has an 8% lower neonlike fraction, down to 10% for the lightest contour. The white regions have less than 10% neonlike fraction. Comparing Figs. 5–7 with Fig. 9, we see that the region of peak gain always falls in the region of the largest neonlike fraction. The difference among the lines is that the 19.6-nm line favors higher densities, since it is driven by direct monopole collisional excitation, and the favorable density region overlaps with the maximum neonlike fraction before the peak optical illumination. During peak illumination the region near critical density is overstripped; therefore not so much neonlike is present, which is why there is a large white region in the middle of the plasma. At this time the neonlike fraction peaks farther from the surface at the lower density and higher temperature, which favors the 23.2 and 23.6 nm lines driven mainly by recombination processes.

5. SUMMARY

We have investigated lasing on the $J = 0{-}1$ and $J = 2{-}1$, $3p{-}3s$ transitions in neonlike germanium. By using slab targets with the prepulse technique, we show that the 19.6-nm, $J = 0{-}1$ laser emission occurs earlier than the pair of $J = 2{-}1$ laser emissions at 23.2 and 23.6 nm, which is the result, as suggested by the XRASER simulation, of the ionization balance in the plasma.

Detailed spatially resolved measurements with 1.2-cm targets show that the $J = 0{-}1$ laser emission at 19.6 nm occurs closer to the target surface than the two $J = 2{-}1$ laser emissions at 23.2 and 23.6 nm. The 23.6 nm laser is the farthest from the target surface. A larger prepulse shifted all lasers farther from the target surface. The combination of the measured temporal and spatial behavior of the lasing explains the measured refraction and beam divergence for the $J = 0{-}1$ versus the $J = 2{-}1$ laser beams in previous experiments. By using a simple model that describes the refraction of the x-ray laser beam during propagation along the target, we compare the LASNEX plus XRASER simulation and the experimental results in detail. Refraction in connection with the hydrodynamics of the plasma is shown to play a key role in governing the beam propagation along the plasma column and hence in producing an effective high gain–length product.

ACKNOWLEDGMENTS

The authors thank the Asterix facilities crew for providing support for the experiments. Yuelin Li was supported by the Alexander von Humboldt Foundation; he thanks S. Witkowski for his hospitality. Georg Pretzler was supported by European Union Programm Human Capital and Mobility CT920015. The work of Joseph Nilsen was performed under the auspices of the U.S. Department of Energy through Lawrence Livermore National Laboratory under contract W-7405-ENG-48. This work was supported in part by the Commission of the European Communities in the framework of the Euratom/Max-Planck-Institut für Plasmaphysik Association.

*Permanent address, Shanghai Institute of Optics and Fine Mechanics, Academia Sinica, P. O. Box. 800-211, Shanghai 201800, China.

REFERENCES

1. D. L. Matthews, P. L. Hagelstein, M. D. Rosen, M. J. Eckart, N. M. Ceglio, A. U. Hazi, H. Medecki, B. J. MacGowan, J. E. Trebes, B. L. Whitten, E. M. Campell, C. W. Hatcher, A. M. Hawryluk, R. L. Kauffman, L. D. Pleasance, G. Rambach, J. H. Scofield, G. Stone, and T. A. Weaver, "Demonstration of soft x-ray amplifier," Phys. Rev. Lett. **54,** 110–113 (1985).
2. T. N. Lee, E. A. Mclean, and R. C. Elton, "Soft x-ray lasing in neonlike germanium and copper plasmas," Phys. Rev. Lett. **59,** 1185–1188 (1987).
3. D. M. O'Neil, C. L. S. Lewis, D. Neely, J. Uhomoibhi, M. H. Key, A. MacPhee, G. J. Tallents, S. A. Ramsden, A. Rogoyski, E. A. McLean, and G. J. Pert, "Characterization of soft x-ray amplification observed in Ne-like germanium," Opt. Commun. **75,** 406–412 (1990).
4. M. Murai, H. Shiraga, G. Yuan, H. Daido, H. Azuma, E. Miura, R. Kodama, M. Takagi, T. Kanabe, H. Takabe, Y. Kato, D. Neely, D. M. O'Neil, C. L. S. Lewis, and A. Djaoui, "Lasing properties of the $J = 0{-}1$ and the $J = 2{-}1$ lines of a neonlike germanium soft-x-ray laser," J. Opt. Soc. Am. B **11,** 2287–2297 (1994).
5. B. L. Whitten, A. U. Hazi, M. H. Chen, and P. L. Hagelstein, "Effect of dielectronic recombination on the kinetics of neonlike selenium," Phys. Rev. A **33,** 3363–2173 (1989).
6. J. Nilsen, "X-ray laser research—consumers of atomic data," Phys. Scri. T **47,** 83–86 (1993).
7. J. Nilsen, J. C. Moreno, B. J. MacGowan, and J. A. Koch, "First observation of lasing at 231 Å in neon-like nickel using the prepulse technique," Appl. Phys. B **57,** 309–311 (1993).
8. J. Nilsen, B. J. MacGowan, L. B. DaSilva, and J. C. Moreno, "Prepulse technique for producing low-Z Ne-like x-ray lasers," Phys. Rev. A **48,** 4682–4685 (1993).
9. J. Nilsen and J. C. Moreno, "Use of the prepulse technique to enhance the weak 18.2-nm laser line in neonlike selenium," Opt. Lett. **19,** 1137–1139 (1994).
10. E. E. Fill, Y. Li, D. Schlögl, J. Steingruber, and J. Nilsen, "Sensitivity of lasing in neonlike zinc at 21.2 nm to the prepulse technique," Opt. Lett. **20,** 374–376 (1995).
11. E. E. Fill, Y. Li, G. Pretzler, D. Schlögl, J. Steingruber, and J. Nilsen, "Study of lasing in low-Z neon-like ions using the prepulse technique," Phys. Scr. **52,** 158–161 (1995).
12. B. Rus, A. Carillon, B. Gauthé, P. Goedtkindt, P. Jaeglé, G. Jamelot, A. Klisnick, A. Sureau, and P. Zeitoun, "Observation of intense soft-x-ray lasing at the $J = 0$ to $J = 1$ transition in neonlike zinc," J. Opt. Soc. Am. B **11,** 564–573 (1994).
13. J. C. Moreno, J. Nilsen, and L. B. Da Silva, "Traveling wave excitation and amplification of neon-like germanium $3p{-}3s$ transitions," Opt. Commun. **110,** 585–589 (1994).
14. J. Nilsen and J. C. Moreno, "Nearly monochromatic lasing at 182 Å in neon-like selenium," Phys. Rev. Lett. **74,** 3376–3379 (1995).
15. R. Kodama, D. Neely, Y. Kato, H. Daido, K. Murai, G. Yuan, A. MacPhee, and C. L. S. Lewis, "Generation of small divergence soft x-ray laser by plasma waveguiding with a curved target," Phys. Rev. Lett. **73,** 3215–3218 (1994).
16. H. Daido, R. Kodama, K. Murai, G. Yuan, M. Takagi, Y. Kato, I. W. Choi, and C. H. Nam, "Significant improvement in the efficiency and brightness of the $J = 0{-}1$ 19.6-nm line of the germanium laser by use of double-pulse pumping," Opt. Lett. **20,** 61–63 (1995).
17. T. Boehly, R. Epstein, R. S. Craxton, M. Russotto, and B. Yaakobi, "X-ray laser in thick foil irradiation geometry," Opt. Commun. **79,** 57–63 (1990).
18. D. Neely, C. L. S. Lewis, D. M. O'Neil, J. Uhomoibhi, M. H. Key, S. J. Rose, G. J. Tallents, and S. A. Ramsden, "Gain scaling relationships for Ne-like Ge slab targets," Opt. Commun. **87,** 231–236 (1992).
19. R. Kodama, D. Neely, L. Dwivedi, M. H. Key, J. Krishan, C. L. S. Lewis, D. M. O'Neil, P. Norreys, G. J. Pert, S. A. Ramsden, G. J. Tallents, J. Uhomoibhi, and J. Zhang, "Time-resolved measurements of the angular distribution of lasing at 23.6 nm in Ne-like germanium," Opt. Commun. **90,** 95–98 (1992).
20. A. Carillon, H. Z. Chen, P. Dhez, L. Dwivedi, J. Jacoby, P. Jaegle, G. Jamelot, J. Zhang, M. H. Key, A. Kidd, A. Klisnick, R. Kodama, J. Krishan, C. L. S. Lewis, D. Neely, P. Norreys, D. M. O'Neil, G. J. Pert, S. A. Ramsden, J. P. Raucort, G. J. Tallents, and J. Uhomoibhi, "Saturated and near-diffraction-limited operation of an XUV laser at 23.6 nm," Phys. Rev. Lett. **68,** 2917–2920 (1992).
21. S. Wang, Y. Gu, G. Zhou, S. Yu, S. Fu, Y. Ni, J. Wu, Z. Zhou, G. Han, Z. Tao, Z. Lin, S. Wang, W. Chen, D. Fan, G. Zhang, J. Sheng, H. Peng, T. Zhang, and Y. Shao, "Experimental investigation of high-gain Ne-like Ge soft-x-ray laser by double-massive-target coupling," J. Opt. Soc. Am. B **9,** 360–368 (1992).
22. S. He, S. Chunyu, Q. Zhang, A. He, H. Shen, Y. Ni, and S. Yu, "Experimental investigation of double-pass amplification of an x-ray laser in neonlike germanium," Phys. Rev. A **46,** 1610–1613 (1992).
23. D. Naccache, A. Decoster, S. Jacquemot, M. Louis-Jacquet, C. J. Keane, B. J. MacGowan, and D. L. Matthews, "Amplification of soft x-rays in Ne-like germanium ions created by 0.53-mm laser light," Phys. Rev. A **42,** 3207–3033 (1990).
24. D. A. Whelan, C. J. Keane, B. J. MacGowan, D. L. Matthews, J. E. Trebes, and M. J. Eckart, "Spatially resolved x-ray laser spectra and demonstration of gain in nickellike systems," in *X-rays from Laser Plasmas,* M. C. Richardson, ed., Proc. SPIE **831,** 275–282 (1987).
25. H. Baumhacker, G. Brederlow, E. Fill, Ch. Schrödter, R. Volk, S. Witkowski, and K. J. Witte, "Performance of the Aster IV iodine laser," Laser Part. Beams **11,** 353–358 (1993).
26. W. Chen, S. Wang, C. Mao, B. Chen, and A. Xu, "Cylinder lens array line focus system for x-ray laser experiments," in *Conference on Laser and Electro-Optics,* Vol. 7 of 1990 OSA Technical Digest Series (Optical Society of America, Washington D.C., 1990), pp. 282–283.
27. Y. Li, G. D. Tsakiris, and R. Sigel, "Self calibration of a thinned, backside illuminated charge-coupled device (CCD)," Rev. Sci. Instrumen. **66,** 80–85 (1995).
28. G. D. Tsakiris, "A soft x-ray streak camera for laser plasma interaction studies," in *Eighteenth International Congress on High Speed Photography and Photonics (August 1988, Xian, Chian),* W. Daheng, ed., Proc. SPIE **1032,** 910–931 (1989).
29. Y. Li, G. Pretzler, and E. E. Fill, "Space-resolved investigation of lasing on the two $J = 0{-}1$, $3p{-}3s$ transitions at 20.5 and 25.5 nm in neon-like iron," Opt. Commun. **119,** 557–562 (1995).
30. G. B. Zimmerman and W. L. Kruer, "Numerical simulation of laser initiated fusion," Comments Plasma Phys. Controlled Fusion **11,** 51–61 (1975).
31. J. Nilsen, "Radiative-hydro modeling and atomic data bases," in *Atomic Processes in Plasmas,* A. Hauer and A. L. Merts, eds., Vol. 168 of AIP Conference Proceedings (American Institute of Physics, New York, 1988), pp. 51–58.
32. P. B. Holden, S. B. Healy, M. T. M. Lightbody, G. J. Pert, J. A. Plowes, A. E. Kingston, E. Robertson, C. L. S. Lewis, and D. Neely, "A computational investigation of the neon-like germanium collisionally pumped laser," J. Phys. B **27,** 341–367 (1994).